Optical and Quantum Electronics (2023) 55:409
https://doi.org/10.1007/s11082-023-04711-1

Surface characterization and linear/nonlinear optical properties of irradiated flexible PVA/ZnO polymeric nanocomposite materials

Nuha Al-Harbi[1] · A. Atta[2] · Rabab K. Sendi[1] · N. A. Althubiti[2] · M. M. Abdelhamied[3]

Received: 10 December 2022 / Accepted: 21 February 2023 / Published online: 12 March 2023

Abstract
In this current study, hydrogen ions of fluence 5×10^{17}, 10×10^{17} as well as 15×10^{17} ions.cm^{-2} were irradiating PVA/ZnO films for applying the irradiated samples in optoelectronics devices. The XRD, SEM, as well as FTIR techniques were used to record the effects of hydrogen ions on the structures, morphologies, as well as functional group of the irradiated films respectively. The FTIR and XRD employed the successful fabricated of the PVA/ZnO composite that made of polyvinyl alcohol (PVA) and zinc oxide nanoparticles (ZnONPs). On the other hand, UV-Vis spectroscopic analysis was utilized to examine optical properties of the PVA/ZnO. The bandgap, absorption edge, as well as Urbach energies of pure and ion-exposed films were calculated via the Tauc's formula. By increasing hydrogen ions to 15×10^{17} ions.cm^{-2}, the Urbach tail increased from 0.36 to 0.43 eV and the optical gap decreased form 2.86 to 2.74 eV. Additionally, the non-linear dispersion properties and optical susceptibilities of pure and irradiated samples were recorded. The irradiated PVA/ZnO samples exhibited enhanced structural and linear/nonlinear optical characteristics, making them suitable for use in optoelectronics.

Keywords PVA/ZnO composites · Ion beam · Structural characteristics · Optical properties · Optoelectronics applications

✉ A. Atta
aamahmad@ju.edu.sa

Nuha Al-Harbi
nfhariby@uqu.edu.sa

[1] Department of Physics, Faculty of Applied Sciences, Umm Al-Qura University, Makkah, Saudi Arabia

[2] Physics Department, College of Science, Jouf University, P.O. Box: 2014, Sakaka, Saudi Arabia

[3] Radiation Physics Department, National Center for Radiation Research and Technology (NCRRT), Atomic Energy Authority (AEA), Cairo, Egypt

1 Introduction

Recently, flexible polymeric composites with novel properties have drawn much interest as materials for optoelectronics implantations (Xu et al. 2021). The polymeric composite materials are attracting more interest due to their unique qualities, such as their geometrical simplicity, lightness, and low cost (Alotaibi et al. 2022). In order to create flexible composite films with conducting nanoparticles, many of researchers were frequently employed in altering their optical characteristics (Abdellah 2021; Mohamed et al. 2022). Various inorganic nano fillers are gaining popularity for a range of energy applications, like light-emitting diode (LED) technology, bioelectronics and microelectronic components (Iqubal 2022).

Conducting ZnO filler has proven for a different applications such as super-capacitors, and conducting inks (Ashour et al. 2021). Moreover, ZnO is the most promising substance for solar cells, optoelectronic components and sensing (Dhatarwal and Sengwa 2021). Due to its high electronic mobility, ZnO is considerable attention as a replacement substance for perovskite photovoltaic-cells (Muthupandeeswari et al. 2021; Zhang 2022). The insertion of ZnONPs in a PVA polymer matrix induced structural alteration that enhances the mechanical performance adaptability of PVA for usage in prospective applications (Folorunso et al. 2022). Due to fascinating characteristics including a large capacity for charge storage and a good dielectric strength, PVA has a wide range of applications (Siwatch et al. 2021). Because PVA has hydroxyl groups attached to C-chain backbones, it can create polymer complexes by bonding (Abdelhamied et al. 2022).

To improving the properties of polymeric composites, surface-modifying techniques like surfaces functionalization and mechanical/thermal/chemical, UV, and ion-beam irradiations are frequently utilized (Althubiti et al. 2023). Additionally, ion beam treatment is selected for altering the polymeric samples over the long time (Alotaibi et al. 2023). Ion-beams are effective method for adapting the features of polymer composite films (Abdelhamied et al. 2021). Ion-beam treating is utilized to enhance surface characteristics of PVA as a result of the influence of ion flux (Alotaibi et al. 2023). In addition, the deposition of ion beam energy alters the physical properties of polymer nanocomposites (Abdeltwab and Atta 2022)when these materials are subjected to low-energy ion beam irradiation. Chain scission, defects, and free radicals were also formed beside these changing properties (Atta et al. 2020). Moreover, ion irradiation is activation the functional group characteristics of the composite materials (Abdeltwab and Atta 2021). The goal of the current experiment is modifying PVA/ZnO samples by subjecting them to various hydrogen ions. The XRD, SEM, and FTIR and UV/Vis investigations were performed to analyze the effects of hydrogen ions on the PVA/ZnO characteristics. The results showed that irradiating PVA/ZnO altered its structural and optical properties are suitable for use in optoelectronic devices.

2 Experimental work

The chemical used are Zinc-nitrate [$Zn(NO_3)_2.6H_2O$, purity of 99.95%], PVA (molecular weight 60.000 to 80.000 and purity 99.5%), as well as ethylene glycol ($C_2H_6O_2$) of purity 98.5%, were provided from Sigma Aldrich. The oxalic acid $C_2H_2O_4$ (98.5%) and zinc acetate dehydrate $Zn(CH_3COO)_2.2H_2O$ (99.95%) were also purchased also from Sigma Aldrich. After that, 1 g of PVA powder id added to 50 ml of distilled water, and the solution was stirred for more than 4 h. Once the PVA solution was ready, 1.5 wt%. of ZnONPs powder was added. The generated sol gel is stirred magnetically and heated for 3 h at 75 °C, then cooled for 10 h at room temperature. The solution is then calcined for 50 min at 380 °C as previously discussed (Abdeltwab and Atta 2021) to form ZnO nanoparticles. Using a casting solution procedure (Althubiti et al. 2022), the solution is casted in cast-glass plates, then, left to dry for 15 h at ambient temp. The composites were eventually taken out of petri plates, then, cut into 1.5×1.5 cm samples for the necessary characterizations. The created films, which have mean thickness of 0.5 mm, are subsequently exposed to hydrogen ions with fluence of 5×10^{17}, 10×10^{17}, as well as 15×10^{17} ions.cm^{-2} (Abdel-Hamid et al. 2020).

The ion source in Fig. 1 is composed of anode and circular cathode, beside an extracting system. This ion source has been previously described (Atta et al. 2021; Abdelhamied et al. 2021). Permanent magnets surround the chamber on two sides, with a small entrance allowing gas to enter the discharge medium. The cathode inside the chamber will emit electrons, which will then gravitate toward the anode. As a consequence, the ionizing atom is increased, which will cause plasma to form. Consequently, extracting electrode is then utilized to collect ion beams. In this work, a gaseous pressure set to 1.8×10^{-4} mbar, beam current intensity was 170 uA, and energy of the extracting ions was around 3 keV.

The structural characteristics of untreated and treated PVA/ZnO films are assessed by XRD (Shimadzu model, XRD-6000, $=1.5406$ Å). By using FT-IR, the function chemical group was identified (Model ATI Mattson, Unicam, UK). Additionally, the morphologies of the changed composites are displayed utilizing SEM (Model JEOL, Japan). Additionally, optical reflections as well as absorption spectrum of the unmodified and exposed composites in the wavelength from 200 μp to 1000 nm are determined utilizing the UV/Vis spectrophotometry (dual-beam JascoV-670). The absorbency A and reflectivity R were typically extracted to calculate the other optical factors.

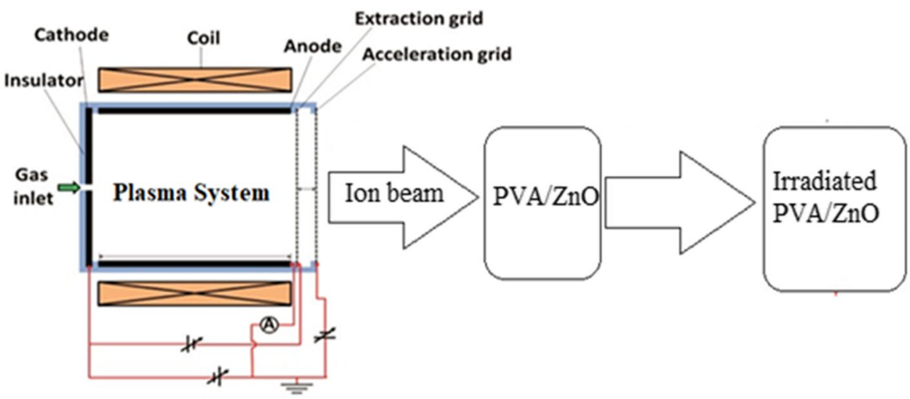

Fig. 1 Electric circuit diagram for cold cathode ion source

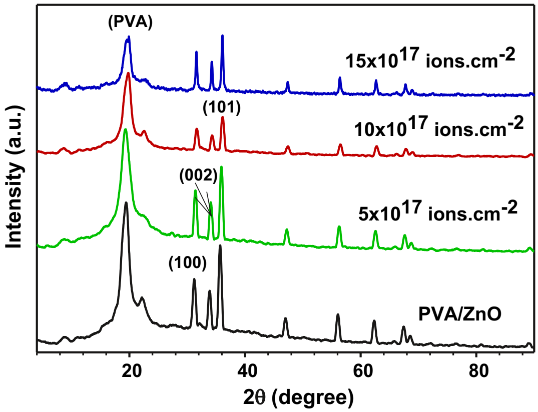

Fig. 2 XRD of non-treated as well as treated PVA/ZnO samples

3 Results and discussions

Figure 2 displays the XRD of pure and treated PVA/ZnO. The untreated PVA/ZnO has three primary peaks at angles of 2θ ~32°, 34.7°, and 36.5°, respectively, which correspond to reflections of the (100), (002), and (101) planes. PVA exhibits a peak about 2θ = 20° (-bdeltwab and Atta 2021; Abdel-Galil et al. 2020). The XRD data show that ZnO/PVA is successfully prepared, with only PVA and ZnO exist as phases in the produced ZnO/PVA. By raising hydrogen ions from5×10^{17} to 15×10^{17} ions.cm^{-2}, the intensity peak of 2θ = 20°for PVA is reduced. This is because the chain scissions as well as the production of free-radicals are induced by increasing ion irradiation (-Atta et al. 2018). Another reason for this reduction in PVA peak intensity is structural alterations in ZnO/PVA chains due to the interactions chains of ZnO and PVA. Additionally, the positional peak has changed noticeably, pointing to a possible physical interaction between the PVA/ZnO chains and ion bombardment. This is due to the interactions between the functional groups in ZnO and PVA as well as hydrogen ions producing the light traps and new defects (Muniz et al. 2016). By increased hydrogen ions exposure, the ZnO/PVA crystallites are also orientated and shifted into positions. This is evidence that hydrogen ions made ZnONPs and PVA chains more miscible.

The crystalline sizes (D) of the ZnO for non-treated as well as treated samples was calculated by (Singh and Bedi 2011).

$$D = \frac{0.94\lambda}{\beta Cos\theta} \quad (1)$$

β is full width maximum, θ is angle of diffraction, and λ denotes wavelength. Furthermore, particle diameter (R) of ZnO for nontreated as well as treated samples is estimated by (Hankare et al. 2003):

$$R = \frac{\lambda}{\sin\beta\cos 2\theta} \quad (2)$$

As shown in Table 1, D as well as R decreases from 32.15 nm as well as 3.65 µm for non-treated PVA/ZnO films to 22.55 nm as well as 2.85 µm for treated PVA/ZnO by 15×10^{17} ions.cm^{-2} respectively. These findings suggest that the composite structure

Table 1 The microstructural features of non-treated and treating PVA/ZnO samples

	D [nm]	R [μm]	δ [10^{-4} lines/ nm^2]	ε [10^{-3}]	g (%)
PVA/ZnO	32.15	3.65	9.6	1.07	0.014
5×10^{17} ions.cm^{-2}	29.85	3.25	11.2	1.16	0.015
10×10^{17} ions.cm^{-2}	26.12	3.05	14.7	1.32	0.017
15×10^{17} ions.cm^{-2}	22.55	2.85	19.6	1.53	0.020

was altered by hydrogen ions. The disordering δof the pure and irradiated films is estimated by (Atta et al. 2022).

$$\delta = \frac{1}{D^2} \tag{3}$$

When PVA/ZnO is exposed to radiation, the dislocation density is increased from 9.6×10^{-4} lines/nm^2 for untreated PVA/ZnO to $19.6*10^{-4}$ lines/nm^2. This is because the structure of the irradiated composite has flaws caused by varying the interplanar spacing. Additionally, the lattice strains (ε) were estimated utilizing Stokes-Wilson formula (Alotaibi et al. 2022)

$$\varepsilon = \frac{\beta}{4\tan\theta} \tag{4}$$

When PVA/ZnO is exposed to radiation, the lattice strains increase from 1.07×10^{-3} for a non-treated sample to 1.53×10^{-3}. Additionally, the distorting factors (g) of the untreated as well as treated samples is computed by (Sabah et al. 2020).

$$g = \frac{\beta}{\tan(\theta)} \tag{5}$$

The distortion values increase with irradiation, going from 14% for pure PVA/ZnO sample to 20% for irradiated samples. Due to the formation of defects and scission by irradiation, the characteristics of the ZnO microstructure alter with the flow of hydrogen ions.

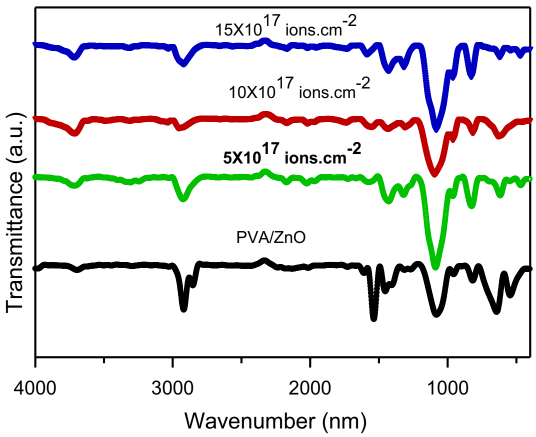

Fig. 3 FTIR of the pure and treated PVA/ZnO.

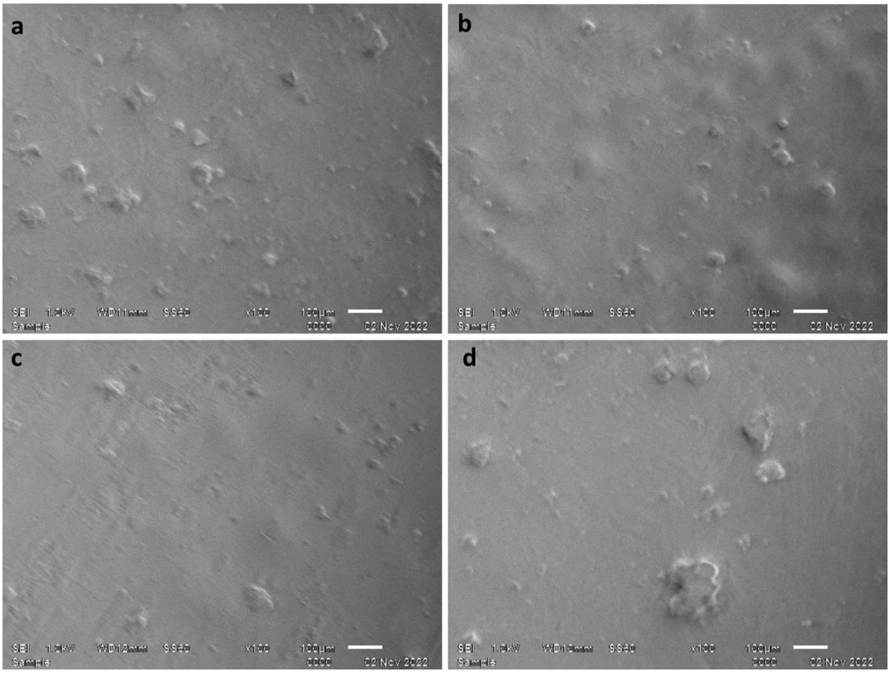

Fig. 4 SEM micrographs of, (**a**) non-treated PVA/ZnO, (**b**) 5×10^{17} ions.cm^{-2}, (**c**) 10×10^{17} ions.cm^{-2}, as well as (**d**) 15×10^{17} ions.cm^{-2}

Additionally, the disordered PVA/ZnO structure is changed by the influence of hydrogen ions. The intermolecular connecting chains for the irradiation films are a further factor affecting the changes in the ZnO microstructure (Sabah et al. 2020).

Figure 3 displays FTIR of non-treated and irradiated ZnO/PVA films. Non-treated ZnO/PVA exhibits a significant broad band in the FTIR that corresponds to the O-H stretch vibrations of the PVA at ~3100–3500 cm^{-1}(Kumaraswamy et al. 2017). While CH_2 asymmetric vibration is at 2850 cm^{-1}, C-H asymmetric vibration is of 2950 cm^{-1}(Atta and Reheem 2022). The bands of C-H and -CH_2 are responsible for the peaks at 1430 cm^{-1} to 1450 cm^{-1}, while –CH_2 wagging is of 1300 cm^{-1}. As a result of hydrogen ions, the intensities of the band 1080 cm^{-1} of the PVA is reduced. The C–C vibrations, that dropped to low peak intensities for the nontreated ZnO/PVA samples, is responsible for another band at 840 cm^{-1}that was found (Atta et al. 2013). Additionally, by raising the fluence of hydrogen ions from 5×10^{17} to 15×10^{17} ions.cm^{-2}, the intensity of irradiated films is significantly lowered and broadened. This is a result of the quantity of defects and chain scission that the irradiation samples produced, which demonstrates the effective miscibility of both ZnO and the polymeric chain in PVA (Alotaibi et al. 2022). A further factor in ZnO's effective miscibility with PVA is the presence of charge transport complexes, which facilitate electron transport between valence and conduction bands (Kayış et al. 2021).

Surface morphologies of the untreated as well as treating PVA/ZnO composite is shown in Fig. 4a, b, c, d. Non-treated PVA/ZnO has granule morphologies with white dots dispersed throughout, as illustrated in Fig. 4(a), indicating the production of ZnO in the PVA matrix (Atta and Abdeltwab 2022). Additionally, Fig.4b, c, d shows SEM images of

Table 2 E_e, E_g as well as E_U values of nontreated as well as treated PVA/ZnO films

Sample	Absorption edge (E_e) (eV)	Band gap (E_g) (eV)	Urbach tail (E_U) (eV)
PVA/ZnO	2.92	3.14	0.33
5×10^{17} ions.cm^{-2}	2.86	3.09	0.36
10×10^{17} ions.cm^{-2}	2.80	3.04	0.41
15×10^{17}ions.cm^{-2}	2.74	3.01	0.43

PVA/ZnO nano-composites treated with 5×10^{17}, 10×10^{17}, as well as 15×10^{17} ions/cm^2, respectively. Following exposure to hydrogen ions, interactions between the PVA chains and the ZnONPs are seen in the SEM pictures. This is brought on by the quantity of flaws and chain scission that the irradiation films created (Rao et al. 2012). This displays the hydrogen ions is improve the miscibility of the ZnO and PVA chains.

3.1 Optical properties

Figure 5a displays the absorbance spectra of untreated and exposed PVA/ZnO. The absorbance of the irradiated PVA/ZnO exhibits behavior that is similar to that of the pure sample. The absorbance of irradiating samples changes as a consequence of the formation of a few homo-polar connections. Using the Beer-Lambert principle (Behera et al. 2020), the absorption coefficients (α) are computed using absorbance values:

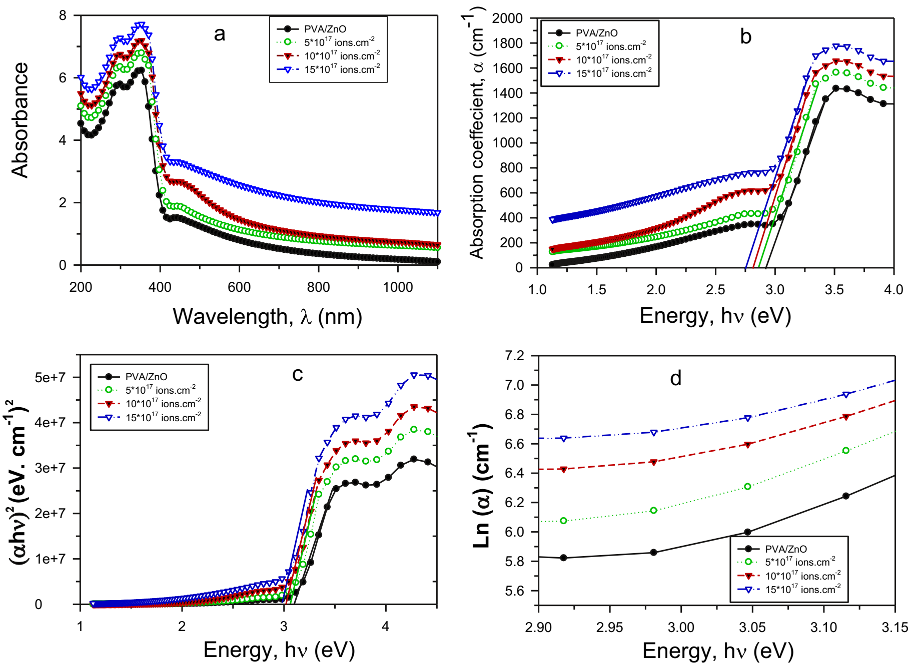

Fig. 5 (**a**) Absorbance A versus λ, (**b**) α versus$h\nu$, (**c**) E_g versus $h\nu$, and (**d**) ln(α) versus$h\nu$, for nontreated as well as treated PVA/ZnO samples

$$\alpha = \frac{2.303\,A}{d} \tag{6}$$

d is thickness and A is the optical absorbance. Figure 5b shows the absorption coefficients (α) of the non-treated as well as treated materials against the incident photon energy ($h\nu$). As the ion beam fluence rises, the absorbance coefficient rapidly increases. This is similar to $As_{40}Se_{45}Bi_{15}$is exposed to 120 MeV Ag ions; the coefficient of absorption rises with increasing ion fluence (Behera et al. 2020). Additionally, Table 2 displays absorption edge E_e of the nontreated and exposed samples computed through extending the straight parts of relative to the photon energies. When PVA/ZnO is treated by 5×10^{17}, 10×10^{17}, as well as 15×10^{17} ions.cm^{-2}, the absorption edge E_e for the untreated sample (2.92 eV) is reduced to 2.86, 2.80, and 2.74 eV, respectively. The absorption edge of the irradiation films is reduced due to the growth of additional homo-polar connections. Free radicals, which lead to the creation of disordered structures as demonstrated by XRD and FTIR, are another factor in the reduction of absorption edge E_e with hydrogen ions.

Using the following formula (Kumaravel et al. 2011), optical bandgap (E_g) is calculated by:

$$\alpha h\nu = A\left(h\nu - E_g\right)^m \tag{7}$$

where $h\nu$ =1240/λ , A is the Tauc constant, as well as $h\nu$is the input energy. Exponent m, that for direct and indirect transitions is equal to m = 1/2 and m = 2, respectively, represents the aspect of electron transitions (Kumaravel et al. 2011). Correlation in-between $(\alpha h\nu)^2$ as well as photon energies is used to compute direct bandgap of both non-treated as well as treated samples. As seen in Fig. 5c and listed in Table 2, the band gapE_g of untreated film is reduced with hydrogen ions. The E_g is reduced from 3.14 eV for PVA/ZnO, to 3.09, 3.04, as well as 3.01 eV, respectively, after exposed to 5×10^{17}, 10×10^{17}, as well as 15×10^{17} ions.cm^{-2}. Similar effect is seen when 120 MeV of Ag^{+9} strikes CdO, and the bandgap is narrowed when the Ag^{+9}fluence is increased (Kumaravel et al. 2011). The ion beam interactions with the composite lead to defects inside the band gap (Zeyada et al. 2012), resulting in a decrease inE_g. Additionally, the accumulation of this limited region between the bands of valence and conduction is another reason for reduction of E_g. The Urbach tail, which is characterized by weakly photon energies, is where optical transmission is most strongly induced between local tail states and broader band states. The incident energy determined by the following formula (Zeyada et al. 2012) determines the Urbach tail energy:

$$\alpha(\nu) = \alpha_o\, e^{h\nu/E_U} \tag{8}$$

where E_U is Urbach tail energy and α_o is a constant number. Figure 5d depicts the connection between photon energy and ln (α) for both non-treated as well as treated samples. As a result, the inverse slope of the straight sections of those graphs was used to compute the band tails for all films (Taha and Saleh 2018) as shown in Table 2. When the PVA/ZnO is subjected to 5×10^{17}, 10×10^{17}, and 15×10^{17} ions.cm^{-2}, respectively, the expected Urbach tails of the nontreated sample (0.33 eV) increased to 0.36 eV, 0.41 eV and to 0.43 eV. For another comparative, the addition of graphene oxide nanosheets (GO) to polyvinyl chloride (PVC) also increases the disorder in the nanocomposite materials, leading to an increase in Urbach tail energy E_u(Taha and Saleh 2018).

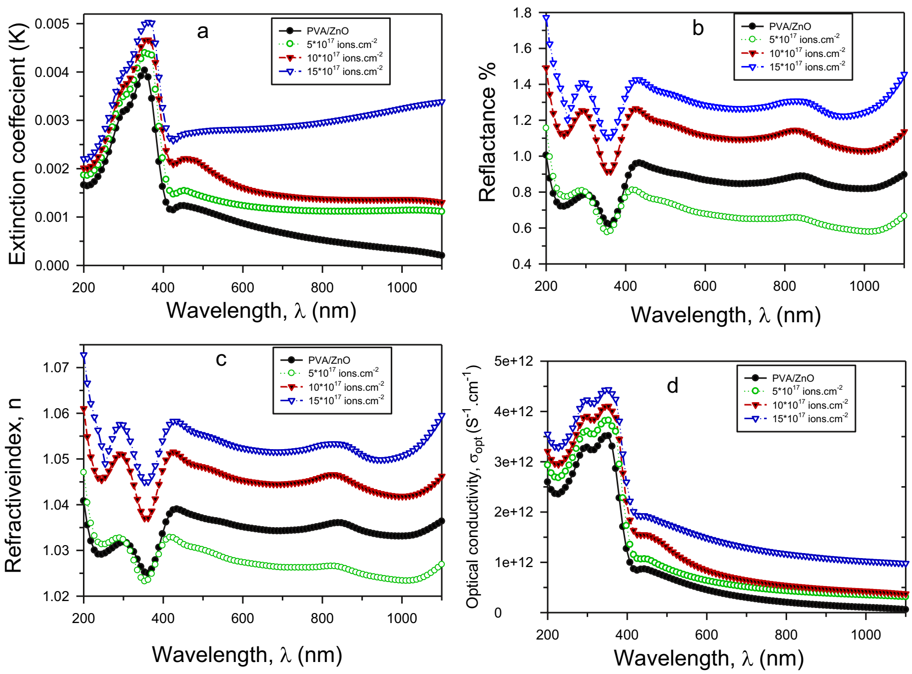

Fig. 6 (**a**) k_o against λ, (**b**) R against λ, (**c**) n against λ, and (**d**) σ_{opt} versus λ, for nontreated as well as treated PVA/ZnO polymers

The extinction coefficient Kis given by (Alrowaili et al. 2021):

$$K = \frac{\alpha\lambda}{4\pi} \tag{9}$$

Figure 6a shows the K varies with photon λ for both untreated and treated PVA/ZnO samples. As can be seen, the increase in defect density caused the k for the irradiated films to modify. Figure 6b shows optical reflectance of nontreated as well as wavelength-treating materials. At higher λ, all samples' reflectance increases and maintains a constant value. Additionally, the reflectance increases with treatment fluences, implying that incident light diffract is minimized. This demonstrates how the disorder has decreased in the treated samples. Additionally, the refractive index (n) is given by 45.

$$n = \frac{(1+R)}{(1-R)} + \sqrt{\frac{4R}{(1-R)^2} - K^2} \tag{10}$$

The refractive indices of the pure and treated PVA/ZnO composite films are shown in Fig. 6c. The refractive indices is progressively increase with an increase in λ. As nontreated sample was subjected to 5×10^{17}, 10×10^{17}, as well as 15×10^{17} ions.cm^{-2}, the index is modified. By forming covalent connections between chains, free radicals alter the density and refractive index of the irradiated films as a result of increased ion irradiation (Banerjee and Kumar 2011; Behera et al. 2019). Moreover, the electron polarization of irradiation PVA/ZnO resulted in an increase in the refractive indices due to the

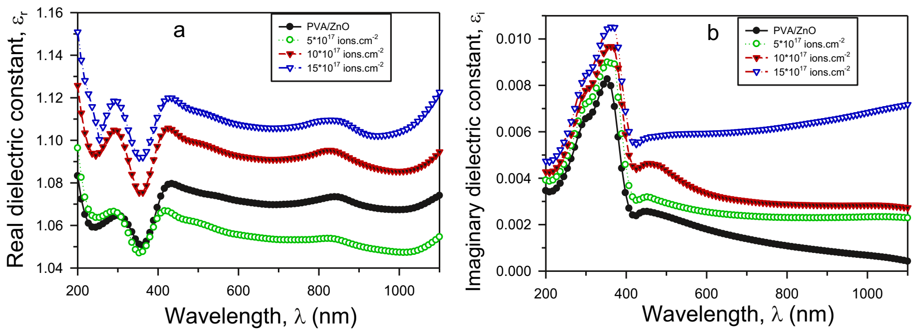

Fig. 7 (**a**) ε_r, and (**b**) ε_i, against λ, for the nontreated and treated PVA/ZnO films

resonance effect. Another factor motivating this change is the nature of the breakdown process itself, which promotes breaking via random interaction. Utilizing relationship (Donya et al. 2020), the optical conductivities$\sigma_{opt}$of non-treated as well as treated samples are computed.

$$\sigma_{opt} = \frac{\alpha n c}{4\pi} \tag{11}$$

Figure 6d shows how the optical conductivity of the nontreated as well as treated samples varies with wavelength. Localized-state concentrations in the band structure, that induce changes in absorption coefficients α, are what cause the optical conductivities of samples to vary with λ. The interaction between PVA and ZnO is also responsible for the improvement in optical conductivity under the impact of hydrogen ions, which indicates that ion irradiation induces a rearrangement in the PVA/ZnO structure. On the other hand, the density of the localized stages and hence the optical conductivity both increase with hydrogen ions. This finding provides more evidence that ZnO and PVA have a good miscibility.One of a substance's most important qualities is its dielectric constant ϵ, which has two components: real ϵ_r and imaginary ϵ_i as indicated in the formula below (Abd El-Rahman et al. 2019):

$$\varepsilon = \varepsilon_r + i\varepsilon_i \tag{12}$$

As indicated in the following formula (Rasheed et al. 2019), the real (ε_r) represents the light dispersion of a substance that is estimated using n and K values:

$$\varepsilon_r = n^2 - K^2 \tag{13}$$

The variations in real component ε_r against λ of the nontreated as well as treated films are shown in Fig. 7a. This increase in ϵ_r with hydrogen ions is because of the creation of covalent links in between numerous chains that rise incident energies losses. Additionally, relation (Alharbi and El-Rahman 2017) is used to calculate the imaginary component ϵ_i that denotes the energy absorption as a result of dipole-moment movements.

$$\varepsilon_i = 2\,n\,k \tag{14}$$

Figure 7b shows the ε_i of pure and irradiated samples as a function of λ. It should be detected that the density and refractive indices of the PVA/ZnO composites were altered by irradiation.

Wemple Di-Domenico's single oscillator paradigm is used to quantify the refractive indices (Al-Zahrani et al. 2015):

$$\frac{1}{n^2-1}=\frac{E_O}{E_d}-\frac{1}{E_O\,E_d}(h\nu)^2 \tag{15}$$

E_o stands for a single energy oscillator, while E_d refers to distributed energy. Figure 8a shows the association between untreated and irradiation samples $(n^2-1)^{-1}$ and$(h\nu)^2$. Both E_o and E_d values are determined by using the intercept and slope of the straight fitting component, respectively. Further, using (El-Nahass et al. 2009), the stationary refractive indices n_o of both untreated and irradiation materials are calculated by:

$$n_o=\left(1+\frac{E_d}{E_O}\right)^{1/2} \tag{16}$$

As a consequence, the relation $\varepsilon_\infty = (n_o)^2$ is used to compute the zero-frequency dielectric constant (ε_∞). The values of E_o and E_d for the nontreated as well as treated PVA/ZnO samples are shown in Table 3. After exposure to hydrogen ions, E_o rises from 2.67 eV for the untreated to 3.24 eV, whereas E_d changed from 0.18 to 0.33 eV. The static index n_o enhanced from 1.03 to 1.5 when exposed to 15×10^{17} ions.cm^{-2}, as seen in Table 3. Oxygen ions have an equivalent effect on MC/PANI/Ag. They demonstrated that an increase in oxygen ions from 0.8×10^{18} to 2.4×10^{18} ions.cm^{-2} resulted in enhanced of the index of from 1.15 to 1.23 (Hamad 2013). Further variables, such the dielectric lattice constants (ε_l), the electron densities (ε_∞) and free carriers' concentrations to effective masses (N/m*) were estimated. The $\varepsilon_r$is estimated using the Spitzer–Fan concept (Hamad 2013):

$$\varepsilon_r=\varepsilon_l-\left(\frac{e^2}{4\,\pi^2\varepsilon_s c^2}\,\frac{N}{m^*}\right)\lambda^2 \tag{17}$$

where ϵ_s is dielectric free space, and c is light speed. Figure 8b displays the relationship between ϵ_r against λ^2 for both nontreated as well as treated films. As shown in Table 3, the ϵ_l and $\frac{N}{m^*}$of the untreated and irradiated samples can be calculated using the slope as well as intercept of the straight sections of the detour, respectively.

The plasma frequencies (W_p) is calculated by (Alwan 2012):

$$W_p=\frac{e^2}{\varepsilon_o}\times\frac{N}{m^*} \tag{18}$$

The amounts of ϵ_l, N/m*, and W_p changed when the pure films were treated by hydrogen fluences of 5×10^{17}, 10×10^{17}, as well as 15×10^{17} ions.cm^{-2}. This adjustment may be connected to the bond length shift that was previously observed in XRD data

Table 3 n_o, ε_∞, E_d, E_o, ε_l, as well as N/m* values of the nontreated as well as irradiated PVA/ZnO

Sample	n_o	ε_∞	E_d (eV)	E_o (eV)	ϵ_l	N/m* x 10^{38} kg^{-1} m^{-3}
PVA/ZnO	1.03	1.06	0.18	2.67	1.063	0.6
5×10^{17} ions.cm^{-2}	1.05	1.08	0.11	2.29	1.060	0.57
10×10^{17} ions.cm^{-2}	1.1	1.21	0.21	2.49	1.097	1.08
15×10^{17} ions.cm^{-2}	1.5	1.10	0.33	3.24	1.111	1.1

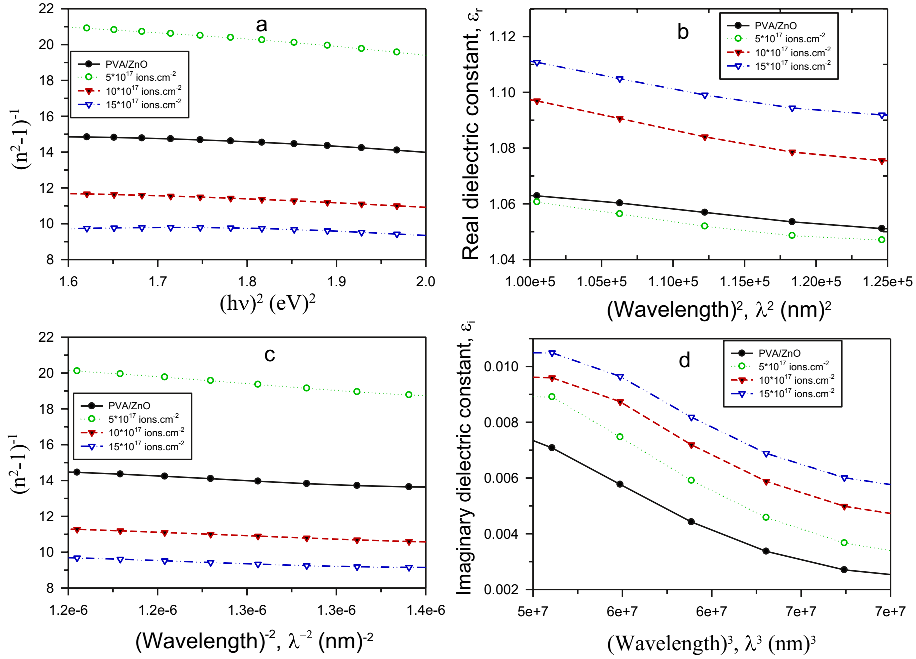

Fig. 8 (**a**) $(n^2\text{-}1)^{-1}$ against $(h\upsilon)^2$, (**b**) ε_r, against λ^2, (**c**) the $(n^2\text{-}1)^{-1}$ against λ^{-2}, and (**d**) ε_i against λ^3, for the nontreated as well as treated PVA/ZnO films

after irradiation. Additionally, the given formula was utilized to compute the refractive indices (n_∞), medium oscillators (λ_o), as well as oscillator lengths (S_o) of the nontreated as well as exposed PVA/ZnO samples (El Sayed et al. 2014):

$$\left(n_\infty^2 - 1\right)/\left(n^2 - 1\right) = 1 - \left(\frac{\lambda_o}{\lambda}\right)^2 \tag{19}$$

The quantities of n_∞ and λ_o are calculated from the slope and intercept of the straight relations of $(n^2-1)^{-1}$ and λ^{-2} as in Fig. 8c, as indicated in Table 4, respectively. The value of λ_o is modified with the influence of hydrogen ions as recorded in Table 4. The addition of ZnO to PVA causes a shift, due to alterations in bond length. In addition, the dipoles contributed to the polarization of the irradiated films is varies with ion beam. Additionally, (Saadeddin et al. 2007) is used to estimate the quantities of S_o:

$$S_o = (n_\infty^2 - 1)/(\lambda_o)^2 \tag{20}$$

Naturally, as the hydrogen beam hits increase, the n_∞ and S_o rise progressively. λ_o amounts for the treated samples decrease on the other hand. However, the Drude idea connects the incident photon wavelength and the imaginary component of the dielectric constant $\epsilon_i$using the given formula (Frumar et al. 2003):

$$\varepsilon_i = \frac{1}{4\pi^3\varepsilon_o}\left(\frac{e^2N}{c^3m^*\tau}\right)\lambda^3 \tag{21}$$

Table 4 W_p, n_∞, λ_o, S_o, and τ of untreated and treated PVA/ZnO composites

Sample	$W_p x10^{12}(sec^{-1})$	n_∞	λ_o (nm)	S_o x 10^6 (m^{-2})	τ x 10^{-7} (sec)
PVA/ZnO	0.17	1.03	519.6	1.1	1.56
5×10^{17} ions.cm^{-2}	0.165	1.02	628.1	0.79	1.25
10×10^{17} ions.cm^{-2}	0.44	1.045	561.2	1.6	1.36
15×10^{17}ions.cm^{-2}	0.35	1.05	458.3	2.1	2.05

Thus, by plotting the relationship between $\epsilon_i$andλ^3, as shown in Fig. 8d, the relaxation time (τ) of the untreated and treated samples is determined. The time relaxation decreases from 1.56x10^{-7} s to 1.25×10^{-7} s with increasing beam fluence to 5×10^{17} ions.cm^{-2}, as shown in Table 4. These investigations showed that when nanocomposite films were bombarded with ions, their optical properties improved, rendering them appropriate for use in higher-speeds optoelectronic implantations.

The given formula (Ticha and Tichy 2002) represents the (NLO) responsivity of a material:

$$P = X^{(1)}E + X^{(2)}E^2 + X^{(3)}E^3 \tag{22}$$

P, $X^{(1)}$, and$X^{(2)}$ correspond the material polarizations, linear susceptibilities, as well as 2nd order NLO susceptibility, whereas$X^{(3)}$ corresponds the 3rd -order NLO susceptibility. The values of $X^{(1)}$ and $X^{(3)}$(Kanis et al. 1991) is computes as follows:

$$X^{(1)} = \frac{(n^2 - 1)}{4\pi} \tag{23}$$

and

$$X^{(3)} = A\left(X^{(1)}\right)^4 \tag{24}$$

The refractive indices are calculated through:

$$n(\lambda) = n_o(\lambda) + n_2\left(E^2\right)$$

where n_o, and n_2 denote linear, and nonlinear indices, correspondingly. NLO refractive indices is computed from NLO susceptibility as well as $n$utilizing (Ali 2021):

$$n_2 = \frac{12\pi X^{(3)}}{n_o}$$

Figures 9a, b show the relationship between $X^{(1)}$ and $X^{(3)}$ with λ for the nontreated as well as treated films, respectively. Both the quantities of $X^{(1)}$and $X^{(3)}$increase as a result of ion bombardment. This increase is linked to the radiation-induced faults (Abomostafa and Abulyazied 2021). Figure9c shows NL refractive indices trend with λ for both non-treated and exposed films. Conspicuously, the amounts of n_2 show same tendency to $X^{(3)}$, gradually increasing as the effects of ion exposure increase. Irradiated PVA/ZnO nanocomposites may be exploited for nonlinear optical applications because developed nonlinear

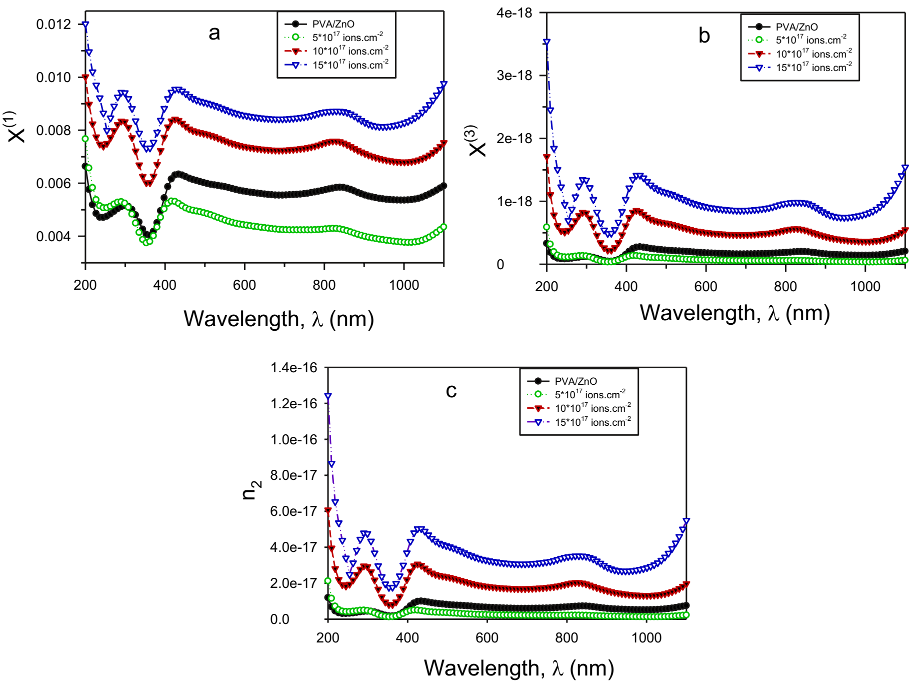

Fig. 9 (**a**) $X^{(1)}$, (**b**) $X^{(3)}$, and (**c**) n_2 against λ for non-treated and treated PVA/ZnO composites

properties of $X^{(3)}$ as well as n_2 [63]. These results showed that the irradiated PVA/ZnO is more appropriate for optoelectronic devices than untreated films.

4 Conclusion

PVA/ZnO films are effectively fabricated by solution casting procedure as indicated by FTIR, XRD and SEM methods. The samples are then irradiated with hydrogen fluence of 5×10^{17}, 10×10^{17} as well as $15x10^{17}$ions.cm^{-2} using broad ion source. The FTIR measures ensure a reduction in the peak intensities of the treated materials. The optical refractive indices, extinction coefficients, and absorption coefficients of non-treated and exposed PVA/ZnO films are determined. The Urbach tails of the untreated sample (0.33 eV) increased to 0.36 eV, 0.41 eV and to 0.43 eV by enhanced hydrogen ions to $5x10^{17}$, 10×10^{17}, and 15×10^{17} ions.cm^{-2}, respectively. An increase in homopolar connections is responsible for the observable change in the bandgap of the exposed samples. Furthermore, the expected optical characteristics of untreated and exposed films were investigated. The results showed that the irradiation films' structural and surface properties were altered in ways that could have wide-ranging implications. Moreover, optical characteristics of the irradiated PVA/ZnO were improved to be more convenient for device applications. Treatment of PVA/ZnO films with hydrogen ions yields superior linear and nonlinear optical properties, suggesting their potential use in optoelectronics.

Author contributions A.-H.A. and S. wrote the results of manuscript text. A.B. and A. reviewed the manuscript. A.-H. and A. prepared the figures. The authors shared in writting the main manuscript.

Funding The authors would like to thank the Deanship of Scientific Research at Umm Al-Qura University for supporting this work by Grant Code: (22UQU4320081DSR01).

Data availability The datasets generated during and/or analysed during the current study are available from the corresponding author on reasonable request.

Declarations

Competing interests The authors declare no competing interests.

References

-Abdel-Galil, A., Atta, A., Balboul, M.R.: Effect of low-energy oxygen ion beam treatment on the structural and physical properties of ZnO thin films. Surf. Rev. Lett. **27**(12), 2050019 (2020)

Abdelhamied, M.M., Abdelreheem, A.M., Atta, A.: Influence of ion beam and silver nanoparticles on dielectric properties of flexible PVA/PANI polymer composite films. Plast., Rubber Compos. **51**(1), 1–12 (2022)

Abdellah, M.Y., et al.: "A novel and highly effective natural vibration modal analysis to Predict Nominal Strength of Open Hole Glass Fiber Reinforced Polymer Composites structure. Polym. **13**(8), 1251 (2021)

Abdeltwab, E., Atta, A.: Plasma-Induced modifications on high density polyethylene and polyethylene terephthalate. ECS J. Solid State Sci. Technol. **11**(4), 043012 (2022)

-Abomostafa, H.M., Abulyazied, D.E.: Linear and nonlinear optical response of nickel Core–Shell@ silica/PMMA nanocomposite film for flexible optoelectronic applications. J. Inorg. Organomet. Polym Mater. **31**(7), 2902–2914 (2021)

Alotaibi, B.M., Al-Yousef, H.A., Alsaif, N.A., Atta, A.: Oxygen beam induced modifications on the structural characteristics and physico-chemical properties of PANI/lead sulfide composite films. Inorg. Chem. Commun. **144**, 109904 (2022)

Alotaibi, B.M., Atta, A., Atta, M.R., Abdeltwab, E., Abdel-Hamid, M.M.: Modifying the optical properties of hydrogen-beam-irradiated flexible PVA polymeric films. Surf. Innovations. **10**, 1–12 (2023)

Althubiti, N.A., Al-Harbi, N., Sendi, R.K., Atta, A., Henaish, A.: Surface characterization and Electrical Properties of Low Energy irradiated PANI/PbS polymeric nanocomposite materials. Inorganics. **11**(2), 74 (2023)

Atta, A., Abdel Reheem, A.M., Abdeltwab, E.: Ion beam irradiation effects on surface morphology and optical properties of ZnO/PVA composites. Surf. Rev. Lett. **27**(09), 1950214 (2020)

Atta, A., Fawzy, Y.H., Bek, A., Abdel-Hamid, H.M., El-Oker, M.M.: Modulation of structure, morphology and wettability of polytetrafluoroethylene surface by low energy ion beam irradiation. Nucl. Instrum. Methods Phys. Res., Sect. B. **300**, 46–53 (2013)

Atta, M.M., Reheem, A.A.: Effect of nitrogen ions on the structural, optical, and thermal properties of polyvinyl alcohol/starch blend. Curr. Appl. Phys. **36**, 43–50 (2022)

-Behera, M., Naik, R., Sripan, C., Ganesan, R., Mishra, N.C.: Influence of Bi content on linear and nonlinear optical properties of As40Se60-xBix chalcogenide thin films. Curr. Appl. Phys. **19**(8), 884–893 (2019)

Folorunso, O., Kumar, N., Hamam, Y., Sadiku, R., Ray, S.S.: Facile solvent/drying fabrication of PVA/PPy/rGO: a novel nanocomposite for energy storage applications. Results Mater **15**, 100295 (2022)

-Iqubal, S.M.: Characterization, Surface Morphology and Microstructure of Water Soluble Colloidal MnO2 Nanoflakes, pp. 1–4. Journal of Umm Al-Qura University for Applied Sciences (2022)

Kumaraswamy, S., Babaladimath, G., Badalamoole, V., Mallaiah, S.H.: Gamma irradiation synthesis and in vitro drug release studies of ZnO/PVA hydrogel nanocomposites. Adv. Mater. Lett. **8**(1), 2–7 (2017)

Mohamed, A.M., Alamri, H.R., Hamad, M.A.: Investigation on Giant Electrocaloric Properties in ferroelectric polymer P (VDF-TrFE)(65/35). Russ. J. Phys. Chem. A. **96**(10), 2259–2264 (2022)

Muthupandeeswari, A., Kalyani, P., Nehru, L.C.: On the effects of high loading of ZnO nanofiller on the structural, optical, impedance and dielectric features of PVA@ ZnO nanocomposite films. Polym. Bull. **78**(12), 7071–7088 (2021)

Sabah, F.A., Razak, I.A., Kabaa, E.A., Zaini, M.F., Omar, A.F.: Characterization of hybrid organic/inorganic semiconductor materials for potential light emitting applications. Opt. Mater. **107**, 110117 (2020)

Singh, I., Bedi, R.: Studies and correlation among the structural, electrical and gas response properties of aerosol spray deposited self assembled nanocrystalline CuO. Appl. Surf. Sci. **257**(17), 7592–7599 (2011)

Abd El-Rahman, -M., Yassien, K.M., Yassene, A.A.: Effect of gamma irradiation on the optical properties of epoxy resin thin films. Optik. **183**, 962–970 (2019)

Abdel-Hamid, H.M., Fawzy, Y.H.A., El-Okr, M.M.: Ion beam and discharge characteristics of cold cathode ion source. Indian J. Pure Appl. Phys. (IJPAP). **5822**(1), 24–30 (2020)

Abdelhamied, M.M., Atta, A., Abdelreheem, A.M., Farag, A.T.M., Sherbiny, E., M. A: Oxygen ion induced variations in the structural and Linear/Nonlinear optical properties of the PVA/PANI/Ag nanocomposite film. Inorg. Chem. Commun. **133**, 108926 (2021)

Abdelhamied, M.M., Atta, A., Abdelreheem, A.M., Farag, A.T.M., Sherbiny, E., M. A: Oxygen ion induced variations in the structural and Linear/Nonlinear optical properties of the PVA/PANI/Ag nanocomposite film. Inorg. Chem. Commun. **133**, 108926 (2021)

-Abdeltwab, E., Atta, A.: Structural and electrical properties of irradiated flexible ZnO/PVA nanocomposite films. Surf. Innov. **40**, 1–9 (2021)

Abdeltwab, E., Atta, A.: Influence of ZnO nanoadditives on the structural characteristics and dielectric properties of PVA. Int. J. Modern Phys. B 2150310. (2021)

Al-Zahrani, -J., El-Hagary, M., El-Taher, A.: Gamma irradiation induced effects on optical properties and single oscillator parameters of Fe-doped CdS diluted magnetic semiconductors thin films. Mater. Sci. Semiconduct. Process. **39**, 74–78 (2015)

Alharbi, -S., El-Rahman, K., Gamma irradiation effects on the linear and nonlinear optical properties of noncrystalline Sb_2S_3 FILMS. Chalcog. Letters.**14**, 652–678 (2017)

Ali, H. E., Abd-Rabboh, H. S., Awwad, N. S., Algarni, H., Sayed, M. A., Abd El-Rehim,A. F., Khairy, Y. (2021). Photoluminescence, optical limiting, and linear/nonlinear optical parameters of PVP/PVAL blend embedded with silver nitrate. Optik, *247*, 167863

Alotaibi, B.M., Al-Yousef, H.A., Alsaif, N.A., Atta, A.: Characterization and optical properties of polymer nanocomposite films for optoelectronic applications. Surf. Innovations. **40**, 1–13 (2022)

Alotaibi, B.M., Atta, M.R., Abdeltwab, E., Atta, A., Abdel-Hamid, M.M.: Surface modifications and optical studies of irradiated flexible PDMS materials. Surf. Innov. 1–10. (2023)

Alotaibi, B.M., Al-Yousef, H.A., Alsaif, N.A., Atta, A.: Characterization and linear/nonlinear optical properties of polymer nanocomposite films for optoelectronics applications. Surf. Innov. 1–11. (2022)

Alrowaili, -Z., Taha, T., El-Nasser, K.S., Donya, H.: Significant enhanced optical parameters of PVA-Y2O3 Polymer Nanocomposite Films. J. Inorg. Organomet. Polym Mater. **31**, 3101–3110 (2021)

Althubiti, N.A., Atta, A., Alotaibi, B.M., Abdelhamied, M.M.: Structural and dielectric properties of ion beam irradiated polymer/silver composite films. Surf. Innov **10**, 1–11 (2022)

Alwan, -T.J.: Gamma irradiation effect on the optical properties and refractive index dispersion of dye doped polystyrene films. Turkish J. Phys. **36**, 377–384 (2012)

Ashour, G., Hussein, M., Sobahi, T.: Nanocomposite containing polyamide and GNS for enhanced properties. Synthesis and characterization, Journal of Umm Al-Qura University for Applied Science 7 (1), (2021) 1–6.Ramesan, M. T. (2022). Development of conductive poly (para-aminophenol)/zinc oxide nanocomposites for optoelectronic devices. Polym. Bull. 1–28. (2021)

Atta, A., Abdeltwab, E.: Influence of ion irradiation on the surface properties of silver-coated flexible PDMS polymeric films. Braz. J. Phys. **52**(1), 1–10 (2022)

Atta, A., Lotfy, S., Abdeltwab, E.: Dielectric properties of irradiated polymer/multiwalled carbon nanotube and its amino functionalized form. J. Appl. Polym. Sci. **135**(33), 46647 (2018)

Atta, A., Althubiti, N.A., Althubiti, S.: Oxygen plasma irradiation-induced surface modifications on HDPE and PET polymeric films.Journal of the Korean Physical Society,1–9. (2021)

Atta, A., Alotaibi, B.M., Abdelhamied, M.M.: Structural characteristics and optical properties of methylcellulose/polyaniline films modified by low energy oxygen irradiation. Inorg. Chem. Commun. 09502. (2022)

Banerjee, -S., Kumar, A.: Swift heavy ion irradiation induced modifications in the optical band gap and Urbach's tail in polyaniline nanofibers. Nucl. Instrum. Methods Phys. Res., Sect. B. **269**, 2798–2806 (2011)

Behera, M., Mishra, N., Khan, S.A., Naik, R.: Influence of 120 MeV Ag swift heavy ion irradiation on the optical and electronic properties of As-Se-Bi chalcogenide thin films. J. Non Cryst. Solids. **544**, 120191 (2020)
Dhatarwal, P., Sengwa, R.J.: Structural, dielectric dispersion and relaxation, and optical properties of multiphase semicrystalline PEO/PMMA/ZnO nanocomposites. Compos. Interfaces. **28**(8), 827–842 (2021)
Donya, -H., Taha, T., Alruwaili, A., Tomsah, I., Ibrahim, M.: Micro-structure and optical spectroscopy of PVA/iron oxide polymer nanocomposites. J. Mater. Res. Technol. **9**, 9189–9194 (2020)
El-Nahass, -M., Farag, A., Abd-El-Salam, F.: Effect of gamma irradiation on the optical properties of nano-crystalline InP thin films. Appl. Surf. Sci. **255**, 9439–9443 (2009)
Frumar, -M., Jedelský, J., Frumarova, B., Wagner, T., Hrdlička, M.: Optically and thermally induced changes of structure, linear and non-linear optical properties of chalcogenides thin films. J. Non-cryst. Solids. **326**, 399–404 (2003)
Hamad, -T.K.: Refractive index dispersion and analysis of the optical parameters of (PMMA/PVA) thin film, Al-Nahrain. J. Sci. **16**, 164–170 (2013)
Hankare, P., Jadhav, A., Bhuse, V., Khomane, A., Garadkar, K.: Chemical deposition of thallium doped cadmium selenide thin films and their characterization. Mater. Chem. Phys. **80**(1), 102–107 (2003)
Kanis, -D.R., Ratner, M.A., Marks, T.J., Zerner, M.C.: Nonlinear optical characteristics of novel inorganic chromophores using the Zindo formalism. Chem. Mater. **3**, 19–22 (1991)
Kayış, A., Kavgacı, M., Yaykaşlı, H., Kerli, S., Eskalen, H.: Investigation of Structural, Morphological, Mechanical, Thermal and Optical Properties of PVA-ZnO Nanocomposites. Glass Phys. Chem. **47**(5), 451–461 (2021)
Kumaravel, R., Ramamurthi, K., Sulania, I., Asokan, K., Kanjilal, D., et al.: Effect of swift heavy ion irradiation on structural, optical and electrical properties of spray deposited CdO thin films. Radiat. Phys. Chem. **80**(3), 435–439 (2011)
Muniz, F.T.L., Miranda, M.A.R., dos Morilla, C., Sasaki, J.M.: The Scherrer equation and the dynamical theory of X-ray diffraction. Acta Crystallogr. Sect. A Found. Adv. **72**(3), 385–390 (2016)
Obasi, -C., Ahmad, A., Ikhioya, I., Ramalan, A., Effect of gamma radiation (60co) on the optical transmittance, energy band gap and absorption coefficient of ZnSe thin films. **40**, 1–26
Rao, -C.V.S., Ravi, M., Raja, V., Bhargav, P.B., Sharma, A.K., Rao, V.N.: Preparation and characterization of PVP-based polymer electrolytes for solid-state battery applications. Iran. Polym. J. **21**, 531–536 (2012)
Rasheed, -H.S., Abbas, I.A., Kadhum, A.J., Maged, H.C.: The effect of gamma irradiation on the optical properties of (PVA-PAA-Al2O3) films, AIP Conf. Proc. AIP Publishing LLC, pp. 020013. (2019)
Saadeddin, -I., Pecquenard, B., Manaud, J.-P., Decourt, R., Labrugère, C., Buffeteau, T., Campet, G.: Synthesis and characterization of single-and co-doped SnO2 thin films for optoelectronic applications. Appl. Surf. Sci. **253**, 5240–5249 (2007)
El Sayed, -A., El-Sayed, S., Morsi, W., Mahrous, S., Hassen, A.: Synthesis, characterization, optical, and dielectric properties of polyvinyl chloride/cadmium oxide nanocomposite films. Polym. Compos. **35**, 1842–1851 (2014)
Siwatch, P., Sharma, K., Manyani, N., Kang, J., Tripathi, S.K.: Characterization of nanostructured nickel cobalt oxide-polyvinyl alcohol composite films for supercapacitor application. J. Alloys Compd. **872**, 159409 (2021)
Taha, -T., Saleh, A.: Dynamic mechanical and optical characterization of PVC/fGO polymer nanocomposites. Appl. Phys. A. **124**, 1–12 (2018)
Ticha, -H., Tichy, L.: Semiempirical relation between non-linear susceptibility (refractive index), linear refractive index and optical gap and its application to amorphous chalcogenides. J. Optoelectron. Adv. Mater. **4**, 381–386 (2002)
Xu, S., Shi, X.L., Dargusch, M., Di, C., Zou, J., Chen, Z.G.: Conducting polymer-based flexible thermoelectric materials and devices: from mechanisms to applications. Prog. Mater. Sci. **121**, 100840 (2021)
Zeyada, -H., El-Nahass, M., El-Shabaan, M.: Gamma-ray irradiation induced structural and optical constants changes of thermally evaporated neutral red thin films. J. Mater. Sci. **47**, 493–502 (2012)
Zhang, H., Liu, J., Shi, F., Li, T., Zhang, H., Yang, D., Zhou, N. (2022). A novel bidirectional fast self-responsive PVA-PNIPAM/LimCsnWO3 composite hydrogel for smart window applications. Chem. Eng. J., *431*, 133353